

Mg²⁺ Impacts the Twister Ribozyme through Push-Pull Stabilization of Nonsequential Phosphate Pairs

Abhishek A. Kognole¹ and Alexander D. MacKerell, Jr.^{1,*}

¹Department of Pharmaceutical Sciences, School of Pharmacy, University of Maryland, Baltimore, Maryland

ABSTRACT RNA molecules perform a variety of biological functions for which the correct three-dimensional structure is essential, including as ribozymes where they catalyze chemical reactions. Metal ions, especially Mg²⁺, neutralize these negatively charged nucleic acids and specifically stabilize RNA tertiary structures as well as impact the folding landscape of RNAs as they assume their tertiary structures. Specific binding sites of Mg²⁺ in folded conformations of RNA have been studied extensively; however, the full range of interactions of the ion with compact intermediates and unfolded states of RNA is challenging to investigate, and the atomic details of the mechanism by which the ion facilitates tertiary structure formation is not fully known. Here, umbrella sampling combined with oscillating chemical potential Grand Canonical Monte Carlo/molecular dynamics simulations are used to capture the energetics and atomic-level details of Mg²⁺-RNA interactions that occur along an unfolding pathway of the Twister ribozyme. The free energy profiles reveal stabilization of partially unfolded states by Mg²⁺, as observed in unfolding experiments, with this stabilization being due to increased sampling of simultaneous interactions of Mg²⁺ with two or more nonsequential phosphate groups. Notably, these results indicate a push-pull mechanism in which the Mg²⁺-RNA interactions actually lead to destabilization of specific nonsequential phosphate-phosphate interactions (i.e., pushed apart), whereas other interactions are stabilized (i.e., pulled together), a balance that stabilizes unfolded states and facilitates the folding of Twister, including the formation of hydrogen bonds associated with the tertiary structure. This study establishes a better understanding of how Mg²⁺-ion interactions contribute to RNA structural properties and stability.

SIGNIFICANCE RNAs are biologically and therapeutically of great emerging interest such that it is critical to understand how RNA molecules fold into biologically active three-dimensional structures. Although experiments yield information on the stabilization of RNA by ions, they are limited in the atomic-level insights they can provide. A combination of conformational and ion enhanced sampling methods is applied to explore the compact intermediate states of RNA and their interactions with Mg²⁺ ions. Results reveal a picture of how Mg²⁺ overall stabilizes short phosphate-phosphate interactions, thereby facilitating the stabilization of RNA, though doing so by both the stabilization and destabilization of specific interactions. The applied method will be applicable to exploring the impact of divalent ions on the conformational heterogeneity of a range of macromolecules.

INTRODUCTION

RNA molecules have highly diverse structures ranging from simple helices to highly heterogeneous folded conformations that are essential for their wide range of cellular functions (1–3). Specifically, ribozymes, a distinct class of enzymes, exhibit complex tertiary structures and catalyze self-cleavage or the cleavage of phosphodiester bonds of substrate RNA, with metal ions typically playing a central role in the catalytic activity (4–6). To assume their tertiary structures, RNAs must

overcome large unfavorable electrostatic interactions associated with their polyanionic phosphodiester backbone (7). To facilitate this, positively charged ions screen the highly negative potential, allowing the RNA secondary structures to collapse into compact tertiary conformations (8–11). Typically divalent ions, most often Mg²⁺, facilitate the formation of tertiary interactions required for the full folding of RNA (12–14). However, the inability to visualize the ions during folding represents a key barrier to understanding the role of divalent ions in folding of RNA (15).

Studies have used classical molecular dynamics (MD) or other theoretical approaches to investigate Mg²⁺-RNA binding, but they were limited to native conformations because of their inability to overcome the issues associated

Submitted August 21, 2019, and accepted for publication January 21, 2020.

*Correspondence: alex@outerbanks.umaryland.edu

Editor: Susan Schroeder.

<https://doi.org/10.1016/j.bpj.2020.01.021>

© 2020 Biophysical Society.

with the Mg²⁺ exchange rates (16–22). The exchange rate of water complexed to Mg²⁺ is on the μ s timescale ($6.7 \times 10^5 \text{ s}^{-1}$), and the exchange rate of Mg²⁺ with phosphate is on the ms timescale ($0.5\text{--}2.5 \times 10^3 \text{ s}^{-1}$) (23), which is beyond the timescale of typical atomistic MD simulations (20,24) such that only limited insights into Mg²⁺-RNA interactions are accessible (25). Alternatively, simulations using coarse-grained models of nucleic acids provided insights into how Mg²⁺ can serve to nucleate the folding of key tertiary interactions with the Mg²⁺-RNA interactions being dominated by specific interactions even in unfolded states (19,26). Reduced models were able to reproduce thermodynamics of Mg²⁺-RNA interactions but were limited to native states (27). Atomistic simulations of unfolding of a pseudoknot at high temperatures showed diverse intermediate states, although divalent ions were absent in those studies (28). Additionally, scientists have worked on improving the force field parameters for positively charged metal ions to better simulate their interactions with biomolecules (29–31). Overall, a detailed picture of the interactions of Mg²⁺ in an explicit solvent environment with partially unfolded states of RNA has not yet been attained.

To investigate the impact of Mg²⁺ on the folding and stabilization of RNA at an atomic level of details, we apply umbrella sampling MD simulations in conjunction with oscillating chemical potential (μ_{ex}) Grand Canonical Monte Carlo (GCMC) sampling of the ion distribution (32). The application of GCMC allows for redistribution of Mg²⁺ ions, thereby addressing the issue of exchange rates, whereas the MD allows the RNA and waters to respond to the changes in ion positions along a folding pathway. The GCMC approach was recently used to sample the distribution of Mg²⁺ ions in a highlighted study on the μ opioid receptor (33,34). The use of GCMC in combination with MD on RNA was first undertaken by Lemkul et al. (35) on four structurally distinct RNAs in their native conformations with restraints on the backbone and was shown to successfully identify experimental Mg²⁺ binding sites as well as predict new ion binding regions. In this study, we extend that approach by combining it with umbrella sampling to sample the distribution of Mg²⁺ around intermediate conformations along a folding pathway. Application of the method reveals an atomic picture of how Mg²⁺ lowers the free energy of partially folded states of RNA by increasing the sampling of specific nonsequential phosphate-phosphate interactions, effectively pulling those phosphates together, through simultaneous interaction between two or more nonsequential phosphates. At the same time, other nonsequential phosphate-phosphate interactions are shown to be destabilized and, therefore, pushed apart to allow for overall stabilization of the tertiary interactions, representing a push-pull mechanism by which Mg²⁺ stabilizes RNA.

The Twister ribozyme was selected for this study based on the availability of a range of structural and biochemical data (6,36–42). Although Twister sequences are extremely

widespread, the crystal structure (PDB: 4OJI) of the ribozyme used in this study is based on Osa-1–4 sequence from *Oryza sativa* (37). Fig. 1 illustrates the secondary and tertiary interactions in Twister. The studied ribozyme has the conserved residues in loops L1, L2, and L4, corresponding to the self-cleavage site and major tertiary interactions (T1 and T2) associated with the double pseudoknot structure of the ribozyme, though it lacks the P3 and P5 stem loops. We additionally refer to the contacts T0 and T3 as tertiary contacts, where T0 consists of a *trans* Watson-Crick (WC)-Hoogsteen basepair U24-A29 situated in loop L4 and T3 consists of basepair C15-G19 situated at the truncated P3 stem loop (37) because we find them important for the ribozyme to assume its tertiary structure (Fig. 1 b). A biophysical study on the same ribozyme, including single-molecule fluorescence resonance energy transfer (FRET) experiments, reported folding kinetics and self-cleavage activity in the presence of Mg²⁺ at various concentrations (39). Results from that study showed Mg²⁺ to facilitate the folding of the RNA, although there was ambiguity around whether Mg²⁺ ions are involved in nucleolytic activity. Roth et al. (36) also showed that Twister is active at very low Mg²⁺ concentrations. It should be noted that both experimental studies included 100 mM KCl in the buffer, which likely also contributes to the screening of the repulsive interactions, potentially allowing Twister to assume the compact intermediate state along with stabilization of secondary interactions (43).

MATERIALS AND METHODS

Potential of mean force calculations

Potential of mean force (PMF) calculations along a folding pathway were performed using umbrella sampling in combination with the oscillating μ_{ex} GCMC/MD method. System preparation involved setting up four Twister simulation systems at 0, 10, 20, and 100 mM MgCl₂, followed by subjecting each system to a classical MD simulation of 200 ns. The final coordinates from each of those simulations were used to generate conformations along the unfolding pathway. This was performed by rapidly unfolding the RNA based on the reaction coordinate (RC) going from 13 to 40 Å in 0.5 Å increments. Each of the subsequent 55 windows was then subjected to a 10-ns MD simulation in the presence of the umbrella potential at the respective RC distances. The final snapshots from these simulations were used to initiate the oscillating μ_{ex} GCMC/MD PMF calculation. This PMF calculation was performed in 1 Å increments from 13 to 40 Å, yielding a total of 28 windows. Specific details for the different aspect of these calculations follow.

MD simulations of the Twister ribozyme were performed in a 90-Å cubic waterbox to accommodate the unfolded conformations at four different concentrations of Mg²⁺ (0, 10, 20, and 100 mM of MgCl₂). The number of atoms in these systems is ~68,000. The 10 mM MgCl₂ system corresponds to the number of Mg²⁺ ions in the Twister crystal structure (PDB: 4OJI, five Mg²⁺ ions), and the initial positions of the ions were based on the crystal structure in this case. The two missing nucleotides in the crystal structure were added by using the internal coordinates in CHARMM (44). In the 20 and 100 mM MgCl₂ systems, all the Mg²⁺ were randomly placed around Twister. In addition to MgCl₂, 100 mM KCl was used in all four systems. The systems were first minimized and equilibrated in CHARMM (44) with harmonic restraints on the backbone and base nonhydrogen atoms with force constants

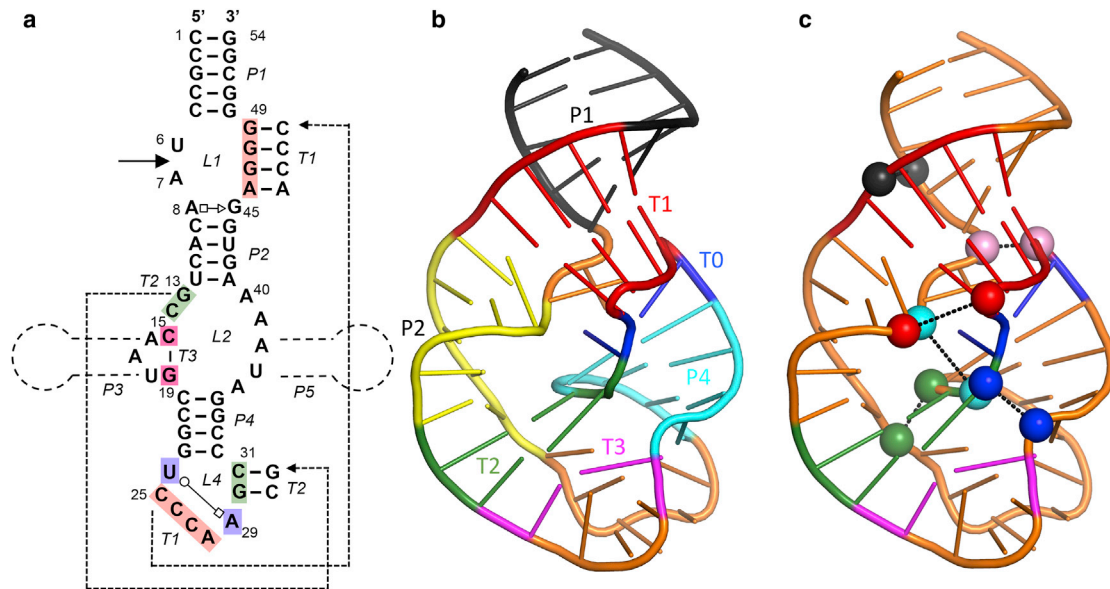


FIGURE 1 Structure of Twister ribozyme and spatially adjacent phosphate pairs. (a) Twister Ribozyme secondary and tertiary contacts are shown. The scissile bond is indicated with a solid arrow, and the omitted P3 and P5 loops are indicated. (b) Contacts are illustrated as cartoons colored as follows: P1, black; P2, yellow; P4, cyan; T0, blue; T1, red; T2, green; T3, magenta; and rest of the RNA, orange. (c) Shown is the Twister ribozyme in its native state with spatially adjacent phosphate pairs that are present in the folded, tertiary structure (*same-colored spheres connected with dashed line*). To see this figure in color, go online.

1 and 0.1 kcal/mol/Å², respectively, for 100 ps in the NPT ensemble with a timestep of 1 fs. CHARMM36 additive force field was used to model RNA and the ions (45–47). Water molecules were modeled by the CHARMM-modified TIP3P force field (48,49). Smooth particle mesh Ewald (PME) method was applied for the calculation of electrostatic interactions with a real-space cutoff of 12 Å (50). The Lennard-Jones potential was force switched to zero between 10 and 12 Å. A Monte Carlo (MC) anisotropic barostat was used to maintain pressure at 1 bar. The lengths of all covalent bonds that involve a hydrogen atom were constrained using the SHAKE algorithm (51). Equilibration was followed by production runs in the NPT ensemble using the Langevin integrator (1 bar, 30°C) with no restraints for 200 ns in OpenMM (52,53) with a time step of 2 fs.

Umbrella sampling MD was used to determine the PMF of breaking the tertiary contacts in Twister (54). The distance between the center of mass of two groups of nucleotides served as the RC (Fig. S1). The RC was selected to globally lead to perturbation of the major tertiary contacts, T1 and T2, in Twister (Fig. 1). The selection also allows for the relative positions of the fluorophores in the FRET study on Twister (39) to be monitored as a function of the RC. To generate unfolded conformations of the RNA, the RC distance was gradually increased in 0.5-Å increments from 15 Å (initial average distance in the native conformation from the 200 ns MD simulations) to 40 Å (partially unfolded conformation), yielding a total of 51 windows. In addition, windows from 15 to 13 Å were generated and sampled in a similar fashion to assure that the true energy minima in the PMFs were identified. The windows were generated using CHARMM by running 10-ps MD simulations at each 0.5-Å step along the RC with a force constant of 5000 kcal/mol/Å² on the RC distance. During this stage, the WC basepairs forming the secondary interactions (P1, P2, and P4) were maintained by restraining the distances between the nonhydrogen atoms involved in all WC basepair hydrogen bonds. A force constant of 4 kcal/mol/Å² was used to apply NOE restraints in CHARMM to maintain the distance between hydrogen bonding atoms of the bases within 2.7–3.0 Å. The final structure in each window was used as the starting structure for the next window. Each window was then simulated in the NPT ensemble for 10 ns in OpenMM (52), in which the COM RC restraint was enforced using PLUMED using a force constant of 4.782 kcal/mol/Å² (2000 kJ/mol/nm²) (55). No restraints were applied on the basepairs of secondary interactions, and the

RNA was allowed to propagate freely. The final frames from these 10-ns simulations were used to start the GCMC/MD simulations for the final PMF calculations. MD simulation conditions were the same in 200-ns production runs of the ribozyme in the native state.

GCMC/MD protocol

A PME oscillating excess chemical potential (μ_{ex}) GCMC algorithm was used to achieve enhanced sampling of the ions around the RNA (32) in conjunction with umbrella sampling to yield the final PMFs. At each window, two separate PMFs were initially calculated. They each involved five cycles of oscillating μ_{ex} GCMC/MD, with each cycle involving a resampling of the ion distribution in the simulation system using oscillating μ_{ex} GCMC, as described below, followed by 10 ns of NPT MD using the above protocol. From the 10-ns MD portions of the 10 oscillating μ_{ex} GCMC/MD cycles, the last 6 ns of data from each of the 10 cycles were collected, yielding a total of 60 ns of sampling in each window from which the free energy profiles were calculated. Calculation of the PMF was performed using the weighted histogram analysis method (56,57). In total, four systems (0, 10, 20, and 100 mM MgCl₂) were subjected to umbrella sampling PMFs, each involving 10 GCMC/MD cycles with 10-ns MD per cycle for each of the 26 windows, yielding a total of 2.6 μs of MD for the Twister ribozyme. Error analysis of the PMFs and other properties extracted from the PMFs was performed by block averaging over five 12-ns blocks in each window and calculating the standard error of mean.

The oscillating μ_{ex} GCMC involved a scheme to oscillate the μ_{ex} of the ions to overcome the low acceptance ratios and avoid using prehydrated Mg²⁺ ions as previously performed (58). In this protocol, we apply MC sampling moves, including insertions, deletions, rotations, and translations of the ions and water. The GCMC sampling protocol was redesigned to resample the ion distribution by deleting and inserting Mg²⁺ ions, whereas K⁺ ions were inserted and deleted simultaneously to maintain the neutral total charge on the system. For systems with no Mg²⁺ ions, the K⁺ and Cl⁻ ions were deleted and inserted together to achieve redistribution of the K⁺ ions. Each single GCMC/MD cycle included seven stages: 1) run

Kognole and MacKerell

20,000 MC steps for deletion of Mg²⁺ and insertion of K⁺; 2) run 80,000 MC steps for rotation and translation of all ions and water; 3) repeat steps 1 and 2 until only one Mg²⁺ is left, and the system is neutral; 4) run 20,000 MC steps for insertion of Mg²⁺ and deletion of K⁺; 5) run 80,000 MC steps for rotation and translation of all ions and water; 6) repeat steps 4 and 5 until the Mg²⁺ concentration is reached, and the system is neutral; and 7) minimize the entire system including RNA, for 5000 steepest descent steps, equilibrated for 100 ps of NVT MD followed by the 10 ns of NPT MD in OpenMM (52). In the PME/GCMC approach, the μ_{ex} values to delete and insert the ions were adopted from the recent study of ionic hydration free energy and are shown in Table S4 (58).

Grid-free energies maps

Occupancies of Mg²⁺ ions were calculated as the number of times a voxel (1 Å cubic unit of volume) around Twister ribozyme was occupied by Mg²⁺ during the simulation. At each window of the PMF, we analyzed 10,000 frames, and all frames were first aligned with respect to the backbone of the ribozyme in the starting conformation for that window. These occupancies were converted to “grid-free energies” (GFE), according to $G = -k_B T \ln(P)$, where P is the probability of occupying a voxel (1 Å cubic unit of volume) on the RNA surface relative to the voxel occupancy of the same species in bulk solution, k_B is the Boltzmann constant, and T is the temperature (303.15 K). A more detailed description of this procedure is provided by Lemkul et al. (35) and elsewhere (59).

RESULTS AND DISCUSSION

In this study, an enhanced sampling method for ion distributions is applied in combination with umbrella sampling to study atomic-level interactions of Mg²⁺ ions with fully and partially folded states of the Twister ribozyme. The protocol implemented includes GCMC simulations to redistribute the Mg²⁺, K⁺, and Cl⁻ ions in the simulation system. The GCMC is followed by minimization and MD simulations to allow the RNA, ions, and water to relax and to obtain conformational sampling of the RNA. Conformational sampling was performed using a computationally accessible one-dimensional RC in which tertiary interactions are lost, allowing the sampling for partially unfolded states of the RNA to investigate their interactions with Mg²⁺. The GCMC/MD approach overcomes the shortcomings of classical MD simulations because of the low exchange rates of Mg²⁺ ions with water and phosphate groups. Notably, the method achieves exchanges of ions around the phosphate groups at the inner-shell level, which is not currently feasible with classical MD. Validation of the method is detailed in [Supporting Materials and Methods](#). The combination of this approach in conjunction with umbrella sampling thus allows a direct relation of the atomic details of Mg²⁺-RNA interactions with the free energies associated with the stabilization of the RNA to be obtained as detailed in the remainder of this manuscript.

Potentials of mean force as a function of MgCl₂ concentration

Twister ribozyme assumes a unique structure with a combination of secondary and tertiary interactions forming a dou-

ble pseudoknot (37). The major tertiary contacts, T1 and T2, are long-range interactions that involve WC basepairing. The nucleotides comprising the individual strands contributing to the two contacts are close in the primary sequence. Accordingly, the center of mass distance between two groups of nucleotides, regions 1 and 2, that approximately each represent half of the folded structure and each include the single strand regions that include T1 and T2 was chosen as the RC (Fig. S1). Regions 1 and 2 include the nucleotides U24 and G54, respectively, to which the individual fluorophores in the single-molecule FRET experiments were covalently linked (39). Along this RC, a folding PMF of the Twister ribozyme was calculated using umbrella sampling with four different concentrations of Mg²⁺. To obtain the impact of Mg²⁺ on the PMFs, the umbrella sampling MD simulations at each RC were periodically stopped, and the ion distribution in the system resampled using the GCMC protocol followed by equilibration and additional production umbrella sampling from which the full PMF was obtained.

The resulting PMFs for Twister at the four MgCl₂ concentrations are shown in Fig. 2a. The free energy surfaces show a sharp minimum at 15.5 Å, corresponding to the fully folded state. The free energy then increases rapidly to an inflection point at ~20 Å, after which the free energy gradually rises out to the fully extended state at RC = 40 Å. From the minima out to 19 Å, the surfaces at the four MgCl₂ concentrations are similar. Beyond 19 Å, the difference between the 0 and 100 mM MgCl₂ surfaces are significant, with the inflection point occurring at ~23 kcal/mol for 100 mM MgCl₂ and ~30 kcal/mol for 0 MgCl₂, with that difference being ~7 kcal/mol throughout the 20–40 Å region of the PMF. The 10 and 20 mM MgCl₂ system PMFs are between the 0 and 100 mM MgCl₂ results beyond 20 Å out to 40 Å. In the remainder of the article, analysis focuses on interpretation of the PMFs in terms of analysis of molecular details of the Mg²⁺-RNA interactions with emphasis on differences between the 0 and 100 mM MgCl₂ systems supported by results from the 10 and 20 mM MgCl₂ systems. Although monotonic differences going from 0 to 100 mM were anticipated, given the limited number of ions in the 10 and 20 mM systems, 5 and 10, respectively, the overall convergence of those systems may require additional sampling. To better understand the results with respect to experimental studies based on FRET and RNase T1 footprinting (39), analysis of the PMFs was undertaken, specifically targeting the molecular phenomena directly related to those experiments.

FRET experiments were based on the fluorophores Cy3 and Cy5; Cy3 was inserted between nucleotides U24 and C25, whereas Cy5 was connected to the 3' termini via a single-stranded DNA spacer (39). In the folded state, the fluorophores are relatively close, allowing for fluorescent energy transfer, whereas upon unfolding, the distance between the fluorophores increases, leading to a loss of energy

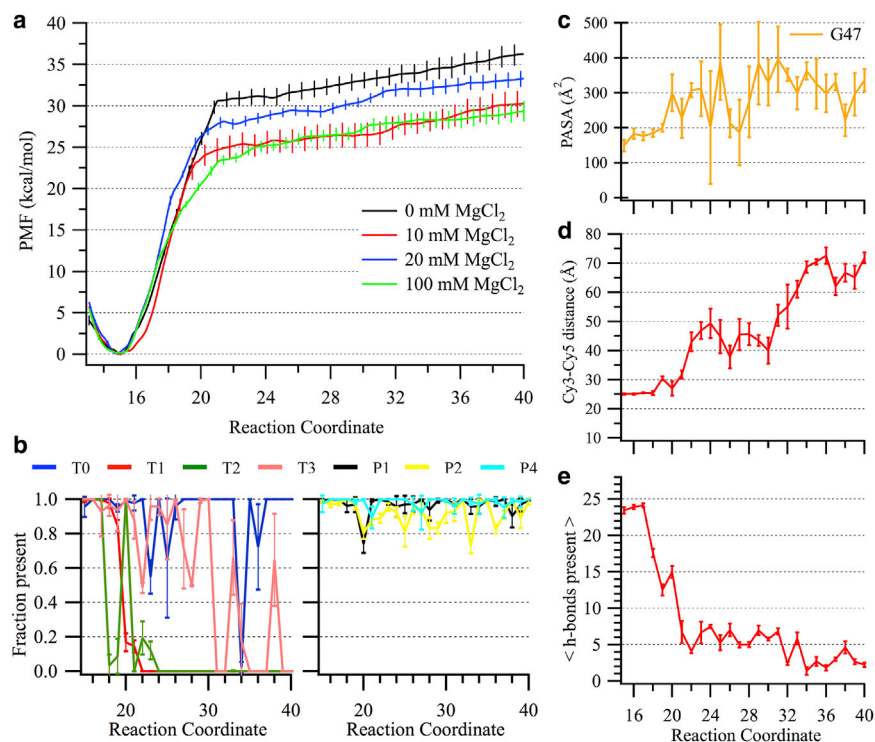


FIGURE 2 Analysis of Twister unfolding simulations. (a) Shown is the potential of mean force (PMF) of Twister ribozyme at different concentrations of MgCl₂ based on the GCMC/MD simulations. The reaction coordinate (RC) corresponds to center of mass distance between two groups of residues that contribute to the T1 and T2 tertiary interactions (Fig. S1). Native state corresponds to RC = 15.5 Å. PMFs were calculated on RC windows at 1-Å intervals from 13 to 40 Å with 60 ns of sampling per window with error bars based on standard error from five 12-ns samples extracted from the full 60 ns of sampling (see Materials and Methods). (b) Shown is the fraction sampled of tertiary (T0, T1, T2, and T3) and secondary (P1, P2, and P4) contacts in Twister present at a given RC for 100 mM MgCl₂ system. A contact is present if the distance between the nucleotides is within three SDs of mean distance for the same contact calculated from the MD simulations in the native state. Fraction is calculated based on the number of frames a contact is present in out of all frames analyzed. (c) Protein-accessible surface area (PASA) for the guanine nucleotide, G47, protected from cleavage by RNase T1 is calculated at each window along the RC. PASA is calculated as the solvent-accessible surface area using a probe radius of 10 Å as previously described (77). (d) Shown is interfluorophore distance (IFD) based

on distance between C4' atoms of Ura 24 and Gua 54 along the RC for Twister. (e) Shown is the number of Watson-Crick (WC) hydrogen bonds present between nucleotides involved in tertiary interactions along the RC. A hydrogen bond was defined by donor-acceptor distance cutoff of 3.0 Å and donor-hydrogen-acceptor angle cutoff of 120°. For (b–e), the data are from the 100 mM MgCl₂ system with results for the other three concentrations provided in the Figs. S2–S6. To see this figure in color, go online.

transfer. To model the spatial relationship of the fluorophores, distances between the C4' atoms of Ura 24 and Gua 54 were measured for each window in the PMFs at all four concentrations (Fig. S4). Shown in Fig. 2 d are the values of the “interfluorophore distance (IFD)” along the RC at 100 mM MgCl₂. Over RC values out to 20 Å and beyond, the IFD does not change, with IFDs beyond 24 Å not occurring until RC = 22 Å, at which point the PMFs have passed their inflection points, attaining energies of 23 kcal/mol or more. Accordingly, significant changes in the actual distance between the fluorophores that would lead to a loss of fluorescence will not occur until this distance along the PMF. In addition, given the length of the linkers on the fluorophores, including the region of single-stranded DNA linking Cy5 to the RNA (Fig. S4), significant unfolding of the RNA may be required to observe the change of fluorescence. This suggests that the FRET experiments may be reporting events that are occurring beyond the global minimal energy wells in the PMFs. A similar interpretation of the experimental results on unfolding based on RNase T1 footprinting experiments may be made (39,60). Shown in Fig. 2 c are calculations at 100 mM MgCl₂ for protein-accessible surface areas (PASAs) of the guanine base, G47, in Twister known to undergo hydrolysis (39). The individual plots for the other guanine bases at all four MgCl₂ concentrations are shown in Fig. S5. Although

the accessibilities of different nucleotides vary, the values for the individual nucleotides do not change significantly to well beyond the inflection point at 20 Å in the PMF. The G47 base is involved in the formation of T1 interaction and a significant increase in PASAs for this base are also observed after the inflection point at 20 Å. This indicates that increased hydrolysis being observed in the footprinting experiments is also not monitoring events associated with transitions from the global free energy minimum to the partially unfolded states (RC = 15–20 Å) but rather associated with events beyond that region that correspond with more global unfolding events (RC = 20–40 Å). Accordingly, interpretation of this simulation results in the context of the FRET data will focus on the regions of the PMF beyond the inflection point at RC = 20 Å. In this region, the 100 mM MgCl₂ system is ~7 kcal/mol more favorable than the 0 mM system, with the 10 and 20 mM results intermediate to those values. This indicates that the presence of 100 mM MgCl₂ lowers the free energy of Twister in these partially unfolded states. Supporting this interpretation is the presence of a small population of the folded state at micromolar Mg²⁺ and a small population of the unfolded state at and above 20 mM Mg²⁺ in the FRET experiments (39). The presence of small populations of the alternate states is consistent with a free energy difference of ~7 kcal/mol versus a difference of over 20 kcal/mol

between the global minima and the inflection at ~ 20 Å in the PMF. Consistent with this model are β parameter results, $\beta_{\text{fold}} = 0.37$ and $\beta_{\text{unfold}} = 0.72$, indicating that the transition to the fully unfolded state observed in the FRET and footprinting experiments occurs closer to the unfolded state (39).

Further support for the experiments monitoring unfolding events beyond those obtained in these calculations may be obtained from the analysis of folding rates. The experimental FRET studies indicate that the folding rate of Twister is under 0.1 s^{-1} (39). Estimates of the folding rate based on the number of nucleotides for Twister, $N = 54$, is $\sim 1200 \text{ s}^{-1}$ (61). From this study, based on an energetic barrier of ~ 20 kcal/mol determined from the PMF (Fig. 2 a) from the minima (folded state (F)) to the inflection point (intermediate state, I, representing an initial unfolded state), an estimate of the equilibrium constant, K_{eq} , for $F \rightleftharpoons I$ based on the van't Hoff equation yields 3.8×10^{-15} . Next, applying an Arrhenius model to calculate the unfolding rate associated with I

(62,63), $k_{F \rightarrow I} = k_o \exp\left(-\frac{E_a}{RT}\right)$, where $E_a = 20$ kcal/mol, and assigning a pre-exponential value, k_o , of $1.3 \times 10^{11} \text{ s}^{-1}$ associated with a harmonic well at the minima of the PMFs, an unfolding rate $k_{F \rightarrow I}$ of $4.9 \times 10^{-4} \text{ s}^{-1}$ is calculated. The folding rate $k_{I \rightarrow F}$ may then be obtained from $K_{\text{eq}} = k_{F \rightarrow I} / k_{I \rightarrow F}$, yielding $1.3 \times 10^{11} \text{ s}^{-1}$. Thus, both the folding rate estimate based on chain length and the PMF, assuming the first intermediate at the inflection point is the unfolded state, are orders of magnitude larger than the experimental estimate of $< 0.1 \text{ s}^{-1}$. These differences further suggest that the FRET and footprinting experiments are monitoring unfolding events that are occurring in the region beyond the inflection point at ~ 20 Å in the PMF that may be associated with the complexity of a double pseudoknot like Twister that differs from that of typical RNAs. In this scenario, the increased population of the folded state observed in the FRET experiments in the presence of Mg^{2+} is more consistent with the free energy of the 100 mM MgCl_2 system being ~ 7 kcal/mol more favorable than 0 mM MgCl_2 . Furthermore, beyond the inflection region at ~ 20 Å in the PMF, there is no indication of a transition to a further unfolded state, and analysis of sampled conformations from the 100 mM MgCl_2 PMF in Fig. 3 show that even at the longest RC = 40 Å, the RNA still contains a significant amount of WC basepairing along with the helical structure associated with the P1 loop. Similar results are obtained at the other three concentrations (Fig. S7). Thus, these results indicate that the loss of all or some of the secondary structural interactions may lead to the unfolded states observed experimentally.

Analysis of the fraction present of the tertiary and secondary contacts (Fig. 1) at the 100 mM MgCl_2 system as a function of the RC is shown in Fig. 2 b, with results for the individual systems shown in Figs. S2 and S3. In the global minima, there is some loss of T2 tertiary interactions, the

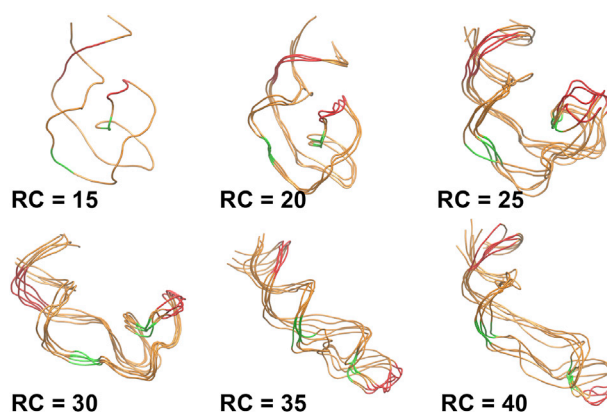


FIGURE 3 Central conformations of top five clusters from 100 mM MgCl_2 PMF simulations at various values of the RC. Backbone root mean-square deviation clustering analysis was performed with a cutoff of 2.5 Å from which the top five clusters of conformations at each window were identified. To see this figure in color, go online.

second largest tertiary contact, in the vicinity of RC = 17–18 Å as the free energy rapidly increases. The larger T1 interaction starts to be perturbed at RC 19 Å, but it is not until beyond the inflection point in the PMF that the T1 interaction is lost, with the remaining T0 and T3 interactions largely maintained through the inflection point out to larger RC values. The secondary contacts, including those in the P1 region, are largely maintained throughout the PMFs (Fig. S3), consistent with a report that secondary structures of RNA are independently stable of the tertiary interactions (64). In the P2 secondary interaction, a *cis*-Hoogsteen-sugar edge pair between A8-G45 is lost during the initial stages when T1 is being broken. In later stages with T1 fully broken, P2 is slightly compromised to stabilize the newly freed bases A46-G49. The inclusion of 100 mM background KCl in this study likely contributes to the stabilization of the secondary interactions throughout the PMF.

Vusurovic et al. present results showing that the crucial T1 interaction, whose formation must precede the P1 stem closing, shows reversible dynamics at physiological Mg^{2+} concentrations (42). However, they did not comment on the formation or unfolding of the T2 tertiary interactions. Overall, both our sampling pathway and the experimental observations from Vusurovic et al. are in agreement that the formation of T1 is one of the last critical steps in folding that ultimately activates self-cleavage of Twister. The importance of P1 formation for folding is still a topic that needs further attention as the Vusurovic study points out that even after self-cleavage and the loss of the P1 duplex, the compact pseudoknot tertiary structure is maintained (42).

To understand the contributions to the energy increase ranging from 23 to 30 kcal/mol upon moving from the global minima to the inflection point in the PMF, the WC hydrogen bonds associated with the tertiary interactions were monitored. The tertiary interactions T1, T2, and T3

correspond to 11, 6, and 3 hydrogen bonds, respectively, associated with seven WC pairs. At 100 mM MgCl₂, upon going from the fully folded state to the inflection point in the PMF, ~80% of the T1 and T2 interactions are lost by 22 Å, corresponding to a loss of 17 hydrogen bonds (Fig. 2 e). Similar changes in the number of hydrogen bonds are observed at all other systems (Fig. S6). Considering that each WC hydrogen bond corresponds to a stabilization free energy ranging from -0.7 to -2 kcal/mol (65,66), their loss corresponds to -12 to -34 kcal/mol, indicating that the deep free energy wells in the PMFs are associated with perturbation of the hydrogen bonds associated with the T1 and T2 tertiary interactions. Analysis of traces of the phosphodiester backbone of Twister at various stages along all four PMFs shows that at RC = 20 and 25 Å, the overall three-dimensional conformation of the RNA is maintained (Figs. 3 and S7). The relatively small change in the overall conformation of the RNA upon going from the global minimum to the region of the inflection point in the PMF further supports the conclusion that the experimental FRET and RNase folding studies are not monitoring the initial loss of tertiary structure but rather a larger scale unfolding event that is not being observed in these calculations. This yields a scenario in which the initial events in unfolding of Twister are dominated by local perturbations of hydrogen bond interactions participating in WC interactions present in the tertiary contacts while the overall structure of the ribozyme is maintained. Once these hydrogen bonds are broken, associated with the change in free energy of 23–30 kcal/mol seen in the PMFs, then larger scale unfolding of the RNA can occur. This unfolding is hypothesized to involve a transition from conformations being sampled beyond the inflection point at 20 Å in the PMFs and a more globally unfolded state. Accordingly, the free energy difference of ~7 kcal/mol between the partially unfolded states in the PMF at 0 and 100 mM Mg²⁺ represent the effective folded state being observed in the experimental studies, consistent with the favoring of the sampling of the folded state in the presence of Mg²⁺ (39,42).

Mg²⁺ distribution and nonsequential phosphate-phosphate interactions

The energetic differences between the 0 and 100 mM MgCl₂ concentrations beyond the PMF inflection point indicate that experimentally relevant partially unfolded states are being sampled. Accordingly, additional analysis focused on understanding the atomic details of the interaction of Mg²⁺ with Twister, including in both the folded state and partially unfolded conformations and how those interactions are leading to a stabilization of the RNA. This analysis is based on the ability of the GCMC/MD protocol to sample a representative ensemble of Mg²⁺ ions around the RNA in both the native and intermediate states.

Analysis of the distribution of Mg²⁺ ions around the RNA was initially undertaken for the folded state based on GFE that are obtained directly from the ion probability distributions as previously performed (35). Fig. 4 presents the distribution of Mg²⁺ around Twister from the RC = 15 Å PMF windows in the presence of 100, 20, and 10 mM MgCl₂, along with the crystallographic ion positions. It is evident that the simulations produce distributions that recapitulate the crystallographic locations of Mg²⁺ even at the lower MgCl₂ concentration. It shows that with decreasing concentration, the Mg²⁺ ions still sample sites observed in the crystal structure, along with additional regions. Fig. 4 c shows that even at 10 mM MgCl₂, Mg²⁺ ions are specifically distributed at crucial intersections, the majority of which correspond to the specific phosphate pairs discussed below. However, at the lower MgCl₂ concentrations, it is likely that the convergence of the ion distribution may require additional sampling, which may impact the free energy surfaces shown in Fig. 2 a such that clear separation of the 0 and 100 mM PMFs are evident with the 10 and 20 mM falling between those curves. Additional studies are required to address this issue.

Further analysis of interactions of the RNA with Mg²⁺ along the RC focused on the presence of spatially adjacent nonbridging phosphate oxygens (NBPOs) of nonsequential nucleotides (i.e., phosphate moieties separated by one or more phosphates in the primary sequence) and their spatial relationship to Mg²⁺. Phosphate-Mg²⁺ interactions, including both direct and indirect coordination, may stabilize both the folded and partially unfolded states by facilitating short phosphate-phosphate interactions. Nonsequential NBPO pairs with a high probability of being within 9 Å of each other were identified as pairs that may simultaneously interact with Mg²⁺ through outer shell interactions (Fig. 5). The cutoff of 9 Å is defined based on radial distribution functions of the distance between NBPO and Mg²⁺ ions (Fig. S8) that show peaks at 1.95, 4.2, and 6 Å, corresponding to direct interaction (inner-shell dehydrated), indirect interaction (outer-shell dehydrated), and diffuse interaction (nondehydrated), respectively (9). Here, we focus on the inner-shell dehydrated and outer-shell dehydrated interactions, which have been classified as strong interactions.

To identify interacting nonsequential NBPOs, adjacent NBPO probability analysis was performed for selected portions of the PMF by merging the data for four consecutive windows (Fig. 5). Analysis of Fig. 5 shows the presence of nonsequential NBPO pairs that are adjacent to each other and that are far apart in the primary sequence as well as a number of NBPO pairs that are adjacent to the diagonal associated with phosphates separated by one or more nucleotides. Table 1 defines six regions of nonadjacent NBPO interactions that occur in the folded state that are identified in the top left panel of Fig. 5. These are shown in Fig. 1 c using the same color scheme as used for the labels in Table 1. Of

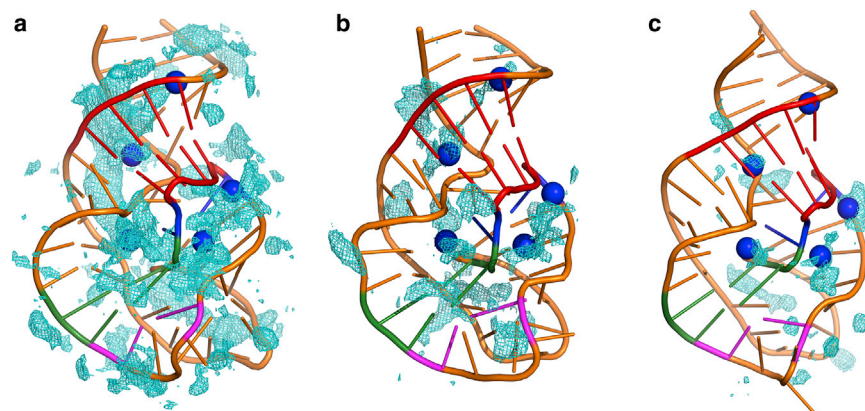


FIGURE 4 (a–c) Occupancy maps for Mg²⁺ ion distribution around native conformation of the Twister ribozyme from the GCMC/MD simulations: (a) 100 mM MgCl₂, (b) 20 mM MgCl₂, and (c) 10 mM MgCl₂. The cutoff for GFE is -2 kcal/mol. The crystallographic positions of Mg²⁺ binding sites are shown in blue spheres after aligning the structures. To see this figure in color, go online.

these, a number are situated around the T1 and T2 tertiary interactions (Table 1). Notable of the pairs present in the folded state is the pair C9-A28 (Fig. 1 c, red spheres) in which A28 is situated at the end of T1, such that this pair coming together facilitates basepair formation in T1. These NBPOs are exposed to the solvent, allowing for Mg²⁺ to simultaneously coordinate with both of them. Additionally, the U6-C25 pair (Fig. 1 c, pink spheres) is situated on the other side of T1, further indicating the importance of bringing phosphates together to stabilize the pseudoknot structure of the ribozyme. Between G3-C5 and A46-G47 (Fig. 1 c, C4-A46, black spheres), there is a range of sites where Mg²⁺ ions may interact with more than two NBPOs. Formation of these pairs appear to stabilize the helical twist of P1 secondary motif while stabilizing nucleotides involved in T1 that may facilitate formation of that contact. The pairs A8-G30 and A8-C31 (Fig. 1 c, cyan spheres) provide an encapsulated space for Mg²⁺ that bridges nucleotides on T1 and T2. NBPO pairs between C32-C33 and A41-G42 (Fig. 1 c, C32-A41, green spheres) are adjacent to and appear to stabilize the T2 interaction. Finally, the

C20-G30 pair (Fig. 1 c, blue spheres) is within 9 Å throughout the majority of the PMF and appears to stabilize nucleotides in the hairpin loop on the end of P4 that participate in both T1 and T2 as well as stabilizing the T0 (U24-A29) and T3 (C15-G19) interactions.

Fig. 6 shows the distribution of Mg²⁺ ions around the phosphate pairs listed in Table 1 using GFE maps at RC = 15 Å in the 100 mM MgCl₂ system. The presence of highly favorable regions of Mg²⁺ sampling directly adjacent to or between all the NBPO pairs is evident. For example, a large region is sampled around the pair 4-46, in which phosphates are lined in parallel fashion with NBPOs facing each other. In general, the presence of Mg²⁺ in the regions surrounding the interacting NBPO pairs will stabilize these interactions, which will lower the free energy of the partially unfolded states. In addition to the NBPO pairs discussed above, there are high probability pairs adjacent to the diagonal of the matrix in the top left panel of Fig. 5. These include 5-7, 8-10, 24-26, 27-29, 29-31, 31-33, and 36-38. These represent kinks in the backbone of the ribozyme that may play an important role in the

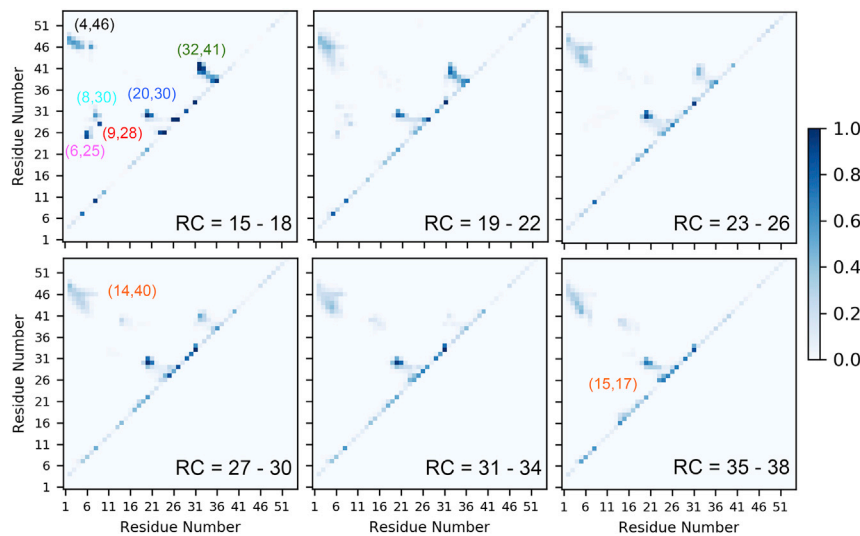


FIGURE 5 NBPO probability matrices from NBPO distance analysis for Twister from the GCMC/MD PMF at 100 mM MgCl₂. The probabilities were averaged over groups of four RC windows. RC = 15–18 corresponds to the fully folded structure. The interactions discussed in the text have been specified with circles. To see this figure in color, go online.

TABLE 1 List of Pairs that Show High Probabilities of Their NBPOs Being within 9.0 Å in the Folded State

Color	Pairs with NBPO Correlation	Adjacent Tertiary Interaction
Black	C4-A46	T1
Red	C9-A28	T0, T1
Cyan	A8-G30	T1
Pink	U6-C25	T0, T1
Green	C32-A41	T2
Blue	C20-G30	T2, T3

Color column corresponds to the pairs shown in Fig. 1 c.

formation of tertiary structure. It has been reported that such kinked structures are stabilized by divalent metal ions (67).

The ability of bidentate chelation of Mg²⁺ ions with sequential phosphate groups has been studied quantum mechanically (68). Intuitively, a bidentate chelation interaction at the A7-A8 pair would be expected to play a role in self-cleavage of the phosphodiester bond between U6-A7. However, stereospecific phosphorothioate substitution studies of the A7 phosphate have shown that inner sphere coordination with divalent ion is not required for catalysis (36,38,40,69,70). Interestingly, the GFE maps in the native state suggest that Mg²⁺ ions highly favor coordination between A8-G30 and A8-C31, and there is minimal Mg²⁺

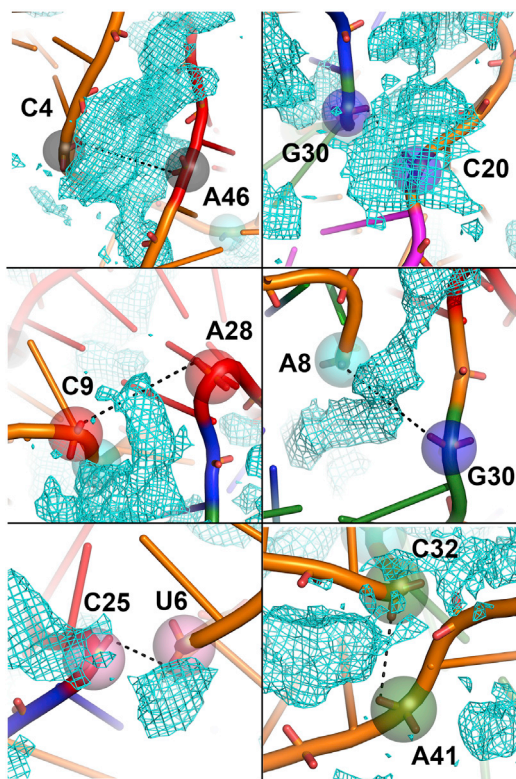


FIGURE 6 Distribution of Mg²⁺ ions around the NBPOs of residue pairs. From the RC = 15 Å, native state of Twister ribozyme (cartoon) from the 100 mM MgCl₂ PMF is shown. The phosphates are represented as same-colored transparent spheres. GFE maps are illustrated as cyan mesh at -2 kcal/mol cutoff. To see this figure in color, go online.

sampling around the A7-A8 phosphate pair (Fig. S9), showing that bidentate chelation of this sequential pair is not occurring in this study, consistent with the experimental observations.

At higher RC values, a number of the pairs present in native state are lost, whereas two new pairs appear. Pairs that are lost correspond to pairs whose individual partners are assigned to the two groups used to define the RC. For example, the 6-25, 8-30, and 9-28 NBPO pairs are lost. New interacting NBPO pairs at long RC values include the 15-17 pair that occurs at RC values greater than 30 Å and the 14-40 pair that first occurs in the 27-30 RC portion of the PMF.

The NBPO probability analysis was also performed for Twister with 0 mM MgCl₂ (Fig. S10). In the absence of Mg²⁺ ions, near the folded state (RC = 15-18), the pattern of NBPO pairs is similar to that at 100 mM MgCl₂, with the 9-28, 8-30, 6-25, and 32-41 pairs being present. However, some differences occur at larger RC values. The group of NBPOs near the 4-46 pair shows lower probabilities with the interaction pattern shifted, and the interaction between 15 and 17 pair at RC = 35-38 is not observed. The similarity of the NBPO pairs in the folded state is consistent with experimental data indicating the ability of Twister to fold and self-cleave at concentrations approaching 0 Mg²⁺ as well as with this PMF (Fig. 2 a), whereas the difference in the larger RC values suggest a role of the ion in stabilizing the partially unfolded states.

To quantify Mg²⁺ ions in the vicinity of the NBPO pairs along the PMF, the probability of Mg²⁺ being present within 6.5 Å of the NBPO atoms of both phosphates in each pair along the RC was calculated. Data are presented for the pairs in Table 1, along with the 14-40 and 15-17 pairs seen in the partially unfolded states. Shown in Fig. 7 are those values as a function of the RC, along with the fraction of the NBPO pair that is within the 9 Å cutoff. It is evident that whenever the NBPOs are close to each other, there is a significant probability of the Mg²⁺ ion being in contact with both of them. The collection of NBPO pairs designated by 4-46 (Fig. 5) was present at fraction probabilities of 0.2 or more along the RC with similar probabilities of Mg²⁺ in their vicinity. Although this interaction is present for the full range of the PMF, it occurs at higher probabilities in the vicinity of the folded state with the Mg²⁺ probability following that trend. With pairs 9-28, 8-30, and 6-25, which involve nucleotides participating in T1, Mg²⁺ ions are interacting with both members, although those interactions are present out to RC = 22 Å. The pair 32-41, which is situated around tertiary contact T2, also has Mg²⁺ extensively coordinated with this NBPO pair. As discussed above, pair 20-30 is maintained along the full PMF with Mg²⁺ ions consistently interacting with the pair. Notably, a similar pattern is observed with the NBPO pairs not present in the folded state. The presence of both the 14-40 and 15-17 pairs in the unfolded states along the PMF is strongly correlated

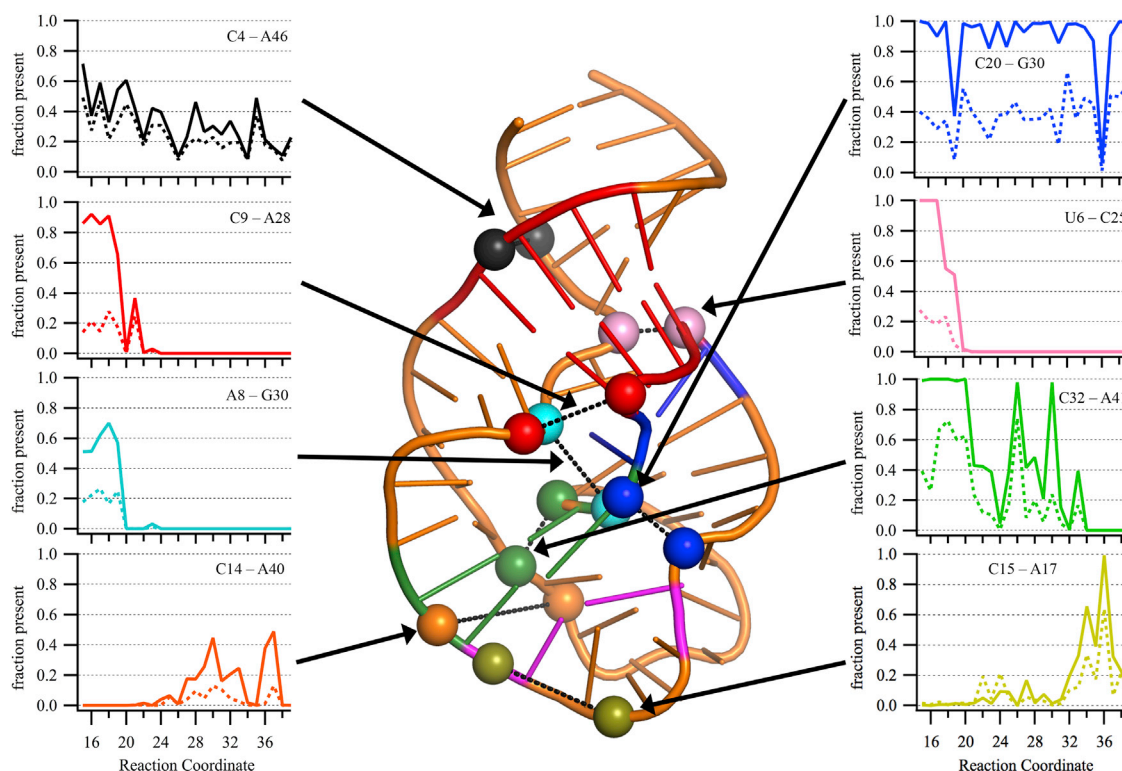


FIGURE 7 Adjacent NBPO pairs in contact with Mg^{2+} ions at 100 mM $MgCl_2$. Shown is the probability of different pairs of nucleotides with NBPOs within 9 Å (solid line) and the probability of a Mg^{2+} ion within 6.5 Å of NBPOs of both phosphates coordinating the two NBPOs (dashed line) along the RC. The arrows point out the positions of NBPO pairs in the Twister structure shown in cartoon, and the phosphate atoms shown as spheres with similar colors. Plots for 20 and 10 mM $MgCl_2$ are provided in Fig. S12. To see this figure in color, go online.

with interactions with Mg^{2+} . Such transient interactions that are facilitated by Mg^{2+} may be important for guiding the RNA along the folding pathway, as previously discussed (19,26).

Toward better understanding the role of NBPO pairs in the partially unfolded RNA, both experimental and computational studies are suggested. Experimentally, phosphorothioate substitutions at these specific pairs could be performed, followed by monitoring of the energetics of unfolded states using FRET or footprinting. Both the 14-40 and 15-17 pair interactions with Mg^{2+} include a significant number of direct interactions (Fig. S11), such that it would be anticipated that the impact of Mg^{2+} on the sampling of the unfolded state would be decreased. Computationally, a repulsive potential between the specific phosphate groups and Mg^{2+} could be applied and the PMF recomputed. This would disallow stabilization of the specific NBPO pairs, thereby altering the energetics of the unfolded states in the presence of Mg^{2+} .

Interesting trends are seen with NBPO pairs that impact the T0 and T3 tertiary contacts. T0 is present throughout the majority of the PMF, though it occurs at a lower probability in the most unfolded states (Fig. 2 b). This contact, which occurs in the L4 loop, is associated with the 20-30 NBPO pair maintained throughout the PMF. A similar trend

is present with the T3 tertiary interaction (15-19 bulge), for which sampling at low levels occurs in the most unfolded states sampled in this study and gradually increasing at smaller RC values (Fig. 2 b). Analysis of the NBPO probability matrices shows the presence of a 15-17 interaction near the diagonal at RC = 35-38, and Fig. 7 shows that Mg^{2+} ions are present around this pair. It suggests that this interaction, which is associated with a kink in the RNA, facilitates the formation of the T3 contact.

To quantify the impact of the presence of Mg^{2+} on the NBPO pairs, the overall probabilities of the presence of those pairs was calculated by integrating over all the individual pair probabilities, excluding those in adjacent phosphates. The results from this analysis are presented in Table 2. Comparison of the results for 100 and 0 mM show the probabilities to be systematically higher throughout the PMF at 100 mM $MgCl_2$, with 10 and 20 mM values typically falling between the 100 and 0 mM values, consistent with the PMFs shown in Fig. 2 a. This difference indicates that whereas the majority of NBPO pairs are present in 0 $MgCl_2$, the presence of Mg^{2+} has an overall stabilizing effect on those interactions. This is consistent with the model of Mg^{2+} stabilizing the repulsion associated with phosphate-phosphate interactions occurring in the tertiary structure (8,71). Thus, the presence

TABLE 2 Summed Probability of the Nonsequential NBPO Pairs Being within the 9.0 Å Cutoff at Various Stages of Unfolding for Systems at Different Mg²⁺ Concentrations

Reaction Coordinate	100 mM	20 mM	10 mM	0 mM
15–18	34.8 ± 0.6	31.1 ± 0.5	35.1 ± 0.4	29.9 ± 0.4
19–22	33.2 ± 1.9	29.7 ± 1.2	30.2 ± 0.6	28.1 ± 1.1
23–26	29.4 ± 1.5	28.7 ± 0.7	30.4 ± 1.7	28.5 ± 0.8
27–30	29.5 ± 1.2	29.9 ± 1.5	28.2 ± 2.3	25.7 ± 0.9
31–34	28.6 ± 1.6	26.4 ± 1.6	28.9 ± 1.0	25.4 ± 0.4
35–38	27.7 ± 1.3	24.1 ± 1.5	27.3 ± 0.9	25.2 ± 0.5

The analysis involves all phosphate-phosphate pairs that are not on adjacent sequential nucleotides in the RNA.

of Mg²⁺ neutralizing phosphate-phosphate repulsion associated with tertiary interactions leads to an overall increase in the sampling of the nonsequential NBPO pairs in Twister. This increased sampling is suggested to contribute to the lowering of the free energy of the RNA as seen in the differences in the PMFs beyond the inflection point where the 100 mM MgCl₂ system is consistently 7 kcal/mol lower than the 0 mM MgCl₂ system.

To investigate the impact of Mg²⁺ on the sampling of the individual NBPO pairs, the summed probabilities were obtained over the different regions of nonsequential NBPO pairs shown in Fig. 5 at 100 mM vs. 0 mM MgCl₂, and the differences were determined. In addition, the contributions from all pairs adjacent to the diagonal were obtained. The differences between the two concentrations are shown in Table 3. Although Mg²⁺ overall stabilizes Twister as well as other RNAs, the results in Table 3 indicate a more complex picture. Several pairs, including 8-30, 32-41, and 20-30, are stabilized in the vicinity of the inflection point in the PMF as well as in the fully folded states as expected. The 4-46 interaction is significantly stabilized throughout the PMF, indicating its impact on the stabilization of the RNA by Mg²⁺ in the full range of conformations studied. In contrast, decreases in the sampling of adjacent NBPO pairs occurs with 9-28 and 6-25 in the inflection and fully folded regions of the PMF, whereas decreases at longer RC values occur with the 32-41, 20-30, and 14-40 pairs. With 14-40, the decreased sampling of close interactions

is consistent with that pair not being present in the folded state, such that its destabilization would facilitate folding. With the 32-41 and 20-30 pairs, the destabilization in the RC = 23-26 region may help to avoid the formation of tertiary interaction too early in the folding process, thereby facilitating the overall folding process. The largest decrease in the sampling of the 9-28 and 6-25 pairs occurs around the inflection point on the PMF at RC = 19–22 Å. As these pairs are directly adjacent to the T1 tertiary contact, their destabilization may facilitate the proper formation of the WC hydrogen bonds that dominate that tertiary contact. Notably, Mg²⁺ is sampling in the vicinity of these pairs (Fig. 6), indicating that despite the presence of Mg²⁺, the increased sampling of other NBPO pairs occurs at the expense of these interactions. It is this balance of interactions that we refer to as the push-pull mechanism for the stabilization of RNA by Mg²⁺, where push-pull refers to the presence of Mg²⁺ plus pulling some phosphate pairs together while simultaneously leading to other NBPO pairs being pushed apart, with the overall outcome being the stabilization of the folded RNA structure despite some individual NBPO pairs being destabilized.

To further investigate the relationship of the 9-28 and 6-25 NBPO pairs to the T1 tertiary contact, correlation analysis was undertaken between the individual NBPO pairs and the number of T1 WC-associated hydrogen bonds in the region of the inflection point in the PMF (RC = 19–21, Table S3). The Pearson correlation coefficients in the case of the 9-28 NBPO pair were –0.35 and –0.62 in 0 and 100 mM MgCl₂, respectively, whereas with the 6-26 NBPO pair, the values were –0.37 to –0.65, respectively. Plots of the NBPO distances versus number of T1 WC hydrogen bonds are presented in Fig. S13. These results show that the shorter NBPO distances correspond to a larger number of T1 hydrogen bonds, as expected given the spatial relationship of the two NBPO pairs to the T1 tertiary contact (Fig. 1). Interestingly, the increase in the magnitude of these correlations in the presence of Mg²⁺ indicates how the ion influences the communication between these two classes of interactions. However, the decrease in the sampling of shorter NBPO distance in the presence of Mg²⁺ (Table 3) indicates that the formation of the T1 hydrogen bonds is

TABLE 3 Difference between the Summed Probabilities at 100 and at 0 mM MgCl₂ for the Individual Nonsequential NBPO Pairs and for the Nonsequential Pairs Adjacent to the Diagonal on Fig. 5

Difference: 100-0 mM MgCl ₂									
RC	pp9-28	pp6-25	pp8-30	pp32-41	pp4-46	pp20-30	pp14-40	pp15-17	Near Diagonal
15–18	–0.08	–0.40	0.20	0.76	2.99	0.93	–0.13	0.11	0.56
19–22	–0.26	–0.71	0.18	1.33	2.74	0.95	0.00	–0.02	0.90
23–26	0.01	0.01	0.02	–0.65	3.65	–1.17	–0.12	–0.13	–0.75
27–30	0.00	0.00	0.00	0.25	3.54	–0.71	–0.40	0.04	1.11
31–34	0.00	0.00	0.00	–0.11	2.84	0.40	–0.73	0.24	0.60
35–38	0.00	0.00	0.00	0.00	3.05	–0.70	0.02	1.10	–0.96

“pp” stands for phosphate-phosphate pair. The near diagonal values were calculated based on the total values shown in Table 2 minus the sum of the NBPO pairs listed in Table 3. Absolute values are shown in Table S1, and standard error in the differences are shown in Table S2.

actually decreased because of the presence of Mg²⁺. This further indicates a complex push-pull type of mechanism in which the presence of Mg²⁺ overall favors the tertiary structure by “pulling” the RNA together while simultaneously leading to a lowered sampling of short 9-28 and 6-25 NBPO pairs by “pushing” them apart in the inflection region of the PMF in which the tertiary contacts are initially forming. This effect is suggested to allow for the T1 hydrogen bonds to sample a wider range of conformational space. Such additional sampling would allow for the formation of the correct pattern of hydrogen bonds associated with the WC interactions that occur in the fully folded state.

CONCLUSIONS

The central observation from these calculations is the overall stabilization of the nonsequential NBPO interactions pairs by Mg²⁺, an observation made in coarse-grained simulations studies of the *Azoarcus* ribozyme (19,26). Notably, in this study, it is shown that Mg²⁺ leads to an overall increased probability of the sampling of specific nonsequential NBPO pairs offering direct evidence of Mg²⁺ contributing to the energetic stabilization of the RNA observed in the PMFs. The most notable such effect occurred in the vicinity of pair 4-46. The region is involved in the stabilization of the P1 helix along with the nucleotides that participate in the T1 tertiary contact. This suggests the Mg²⁺ is specifically interacting with the RNA to stabilize the conformation of this region, thereby facilitating formation of the T1 contact upon full folding of the RNA. Interestingly, Mg²⁺ is not seen in the P1 region of Twister in the crystallographic structures PDB: 4OJI and PDB: 4RGE (37,41), whereas the FRET studies on both sequences show conflicting results on the importance of this stem in folding and activity as recently discussed and addressed by Gaines et al. (39,40,42).

Other individual NBPO pairs are stabilized or destabilized to varying extents consistent with Mg²⁺ facilitating RNA folding and stability in a sequence-specific fashion. Decreased sampling of specific nonsequential NBPO pairs in the presence of Mg²⁺ is a somewhat surprising result (Table 3). For example, in the vicinity of the inflection region of the PMF and in the folded states, the sampling of the 9-28 and 6-25 pairs is decreased by Mg²⁺ as also occurs in the partially unfolded states with the 14-40 pair. This shows that the specific effects of Mg²⁺ include destabilization of selected nonsequential NBPO pairs as other phosphate-phosphate interactions are being stabilized. In the case of 14-40, as this interaction is not present in the folded states, its destabilization would facilitate access to those folded states. In the case of 9-28 and 6-25, the results indicate that partial destabilization of the pairs facilitates the proper formation of the hydrogen bonds associated with the WC interactions of the T1 tertiary contact such that Mg²⁺ allows Twister to break and form the hydrogen bonds associated with the T1 tertiary contact. This appears to contribute to the smooth transition in

the PMFs around the inflection point in the presence of Mg²⁺ versus in its absence where a sharp transition occurs (Fig. 2 a). These results indicate a push-pull scenario of Mg²⁺ stabilization of RNA in which, despite the general neutralization of phosphate-phosphate repulsion, the nature of the Mg²⁺ interactions leads to lowered sampling of specific nonsequential phosphate pairs that are effectively being pushed apart to facilitate pulling the overall structure together, yielding overall stabilization of the RNA. Although we anticipate that the identified push-pull mechanism contributes to the stabilization of other RNAs by Mg²⁺, given the unique features of Twister in which Mg²⁺ concentrations approaching zero still allow for self-cleavage, it would appear that the role of Mg²⁺ in RNA structure and function varies for different systems.

The deep global minima observed in these PMFs, which are largely insensitive to ion concentration, may explain the ability of Twister to self-cleave at very low Mg²⁺ concentrations and that sampling of the folded state required for catalysis may occur in all conditions. We recognize that the role of the background of 100 mM KCl (72), included in this study to be consistent with the experimental study, requires further attention to understand the role of monovalent ions in RNA folding. We have provided analyses indicating that the experimental FRET and RNase T1 footprinting studies are monitoring unfolding events at RC distances beyond the inflection point at 20 Å in the PMFs. Accordingly, this RC used to define the folding landscape is not accessing the fully unfolded conformations. However, the one-dimensional RC selected for this study has allowed investigation of the impact of Mg²⁺ on compact intermediates and partially unfolded states using a novel GCMC ion sampling approach. Additional studies are needed to address the issue of choosing the best RC to investigate the full unfolding profile of Twister and recent advances in machine learning may help solve this problem (73). Overall, the study implemented a novel GCMC approach to investigate the highly complex problem of RNA folding and provides new insights on the impact of Mg²⁺ ions on both the folded and unfolded states of the Twister ribozyme.

SUPPORTING MATERIAL

Supporting Material can be found online at <https://doi.org/10.1016/j.bpj.2020.01.021>.

AUTHOR CONTRIBUTIONS

A.D.M. conceived the overall project. A.A.K. and A.D.M. designed the methods and models for simulations. A.A.K. built and performed the simulations. A.A.K. and A.D.M. analyzed the data and wrote the manuscript.

ACKNOWLEDGMENTS

We thank Dr. Sarah Woodson and Dr. Darrin York for helpful discussions. A.D.M. is co-founder and CSO of SilcsBio.

We thank the National Institutes of Health (GM131710) for financial support for this work and the Computer-Aided Drug Design Center at the University of Maryland Baltimore for computing time.

SUPPORTING CITATIONS

References (74–76) appear in the Supporting Material.

REFERENCES

1. Fedor, M. J. 2002. The role of metal ions in RNA catalysis. *Curr. Opin. Struct. Biol.* 12:289–295.
2. Cech, T. R., and J. A. Steitz. 2014. The noncoding RNA revolution—trashing old rules to forge new ones. *Cell.* 157:77–94.
3. Morris, K. V., and J. S. Mattick. 2014. The rise of regulatory RNA. *Nat. Rev. Genet.* 15:423–437.
4. Pyle, A. M. 1993. Ribozymes: a distinct class of metalloenzymes. *Science.* 261:709–714.
5. Usman, N., L. Beigelman, and J. A. McSwiggen. 1996. Hammerhead ribozyme engineering. *Curr. Opin. Struct. Biol.* 6:527–533.
6. Gaines, C. S., and D. M. York. 2016. Ribozyme catalysis with a twist: active state of the twister ribozyme in solution predicted from molecular simulation. *J. Am. Chem. Soc.* 138:3058–3065.
7. Tinoco, I., Jr., and C. Bustamante. 1999. How RNA folds. *J. Mol. Biol.* 293:271–281.
8. Draper, D. E., D. Grilley, and A. M. Soto. 2005. Ions and RNA folding. *Annu. Rev. Biophys. Biomol. Struct.* 34:221–243.
9. Draper, D. E. 2004. A guide to ions and RNA structure. *RNA.* 10:335–343.
10. Heilman-Miller, S. L., D. Thirumalai, and S. A. Woodson. 2001. Role of counterion condensation in folding of the Tetrahymena ribozyme. I. Equilibrium stabilization by cations. *J. Mol. Biol.* 306:1157–1166.
11. Woodson, S. A. 2010. Compact intermediates in RNA folding. *Annu. Rev. Biophys.* 39:61–77.
12. Fang, X., T. Pan, and T. R. Sosnick. 1999. A thermodynamic framework and cooperativity in the tertiary folding of a Mg²⁺-dependent ribozyme. *Biochemistry.* 38:16840–16846.
13. Heilman-Miller, S. L., J. Pan, ..., S. A. Woodson. 2001. Role of counterion condensation in folding of the Tetrahymena ribozyme. II. Counterion-dependence of folding kinetics. *J. Mol. Biol.* 309:57–68.
14. Misra, V. K., R. Shiman, and D. E. Draper. 2003. A thermodynamic framework for the magnesium-dependent folding of RNA. *Biopolymers.* 69:118–136.
15. Pyle, A. M. 2002. Metal ions in the structure and function of RNA. *J. Biol. Inorg. Chem.* 7:679–690.
16. Tsui, V., and D. A. Case. 2001. Calculations of the absolute free energies of binding between RNA and metal ions using molecular dynamics simulations and continuum electrostatics. *J. Phys. Chem. B.* 105:11314–11325.
17. Auffinger, P., L. Bielecki, and E. Westhof. 2003. The Mg²⁺ binding sites of the 5S rRNA loop E motif as investigated by molecular dynamics simulations. *Chem. Biol.* 10:551–561.
18. Kirmizialtin, S., S. A. Pabit, ..., R. Elber. 2012. RNA and its ionic cloud: solution scattering experiments and atomically detailed simulations. *Biophys. J.* 102:819–828.
19. Denesyuk, N. A., and D. Thirumalai. 2015. How do metal ions direct ribozyme folding? *Nat. Chem.* 7:793–801.
20. Ucisk, M. N., P. C. Bevilacqua, and S. Hammes-Schiffer. 2016. Molecular dynamics study of twister ribozyme: role of Mg(2+) ions and the hydrogen-bonding network in the active site. *Biochemistry.* 55:3834–3846.
21. Giambaşu, G. M., D. A. Case, and D. M. York. 2019. Predicting site-binding modes of ions and water to nucleic acids using molecular solvation theory. *J. Am. Chem. Soc.* 141:2435–2445.
22. Cunha, R. A., and G. Bussi. 2017. Unraveling Mg²⁺-RNA binding with atomistic molecular dynamics. *RNA.* 23:628–638.
23. Allnér, O., L. Nilsson, and A. Villa. 2012. Magnesium ion-water coordination and exchange in biomolecular simulations. *J. Chem. Theory Comput.* 8:1493–1502.
24. Li, P., B. P. Roberts, ..., K. M. Merz, Jr. 2013. Rational design of particle mesh Ewald compatible Lennard-Jones parameters for +2 metal cations in explicit solvent. *J. Chem. Theory Comput.* 9:2733–2748.
25. Hayes, R. L., J. K. Noel, ..., K. Y. Sanbonmatsu. 2012. Magnesium fluctuations modulate RNA dynamics in the SAM-I riboswitch. *J. Am. Chem. Soc.* 134:12043–12053.
26. Hori, N., N. A. Denesyuk, and D. Thirumalai. 2019. Ion condensation onto ribozyme is site specific and fold dependent. *Biophys. J.* 116:2400–2410.
27. Hayes, R. L., J. K. Noel, ..., J. N. Onuchic. 2014. Reduced model captures Mg(2+)-RNA interaction free energy of riboswitches. *Biophys. J.* 106:1508–1519.
28. Zhang, Y., J. Zhang, and W. Wang. 2011. Atomistic analysis of pseudo-knotted RNA unfolding. *J. Am. Chem. Soc.* 133:6882–6885.
29. Panteva, M. T., G. M. Giambaşu, and D. M. York. 2015. Force field for Mg(2+), Mn(2+), Zn(2+), and Cd(2+) ions that have balanced interactions with nucleic acids. *J. Phys. Chem. B.* 119:15460–15470.
30. Yoo, J., and A. Aksimentiev. 2012. Improved parametrization of Li+, Na+, K+, and Mg2+ ions for all-atom molecular dynamics simulations of nucleic acid systems. *J. Phys. Chem. Lett.* 3:45–50.
31. Casalino, L., G. Palermo, ..., A. Magistrato. 2017. Development of site-specific Mg(2+)-RNA force field parameters: a dream or reality? Guidelines from combined molecular dynamics and quantum mechanics simulations. *J. Chem. Theory Comput.* 13:340–352.
32. Lakkaraju, S. K., E. P. Raman, ..., A. D. MacKerell, Jr. 2014. Sampling of organic solutes in aqueous and heterogeneous environments using oscillating excess chemical potentials in grand canonical-like Monte Carlo-molecular dynamics simulations. *J. Chem. Theory Comput.* 10:2281–2290.
33. Hu, X., D. Provasi, ..., M. Filizola. 2019. Mechanism of μ -opioid receptor-magnesium interaction and positive allosteric modulation. *Biophys. J.* Published online October 14, 2019. <https://doi.org/10.1016/j.bpj.2019.10.007>.
34. MacKerell, A. D., Jr. 2019. Ions everywhere? Mg²⁺ in the μ -opioid GPCR and atomic details of their impact on function. *Biophys. J.* Published online October 22, 2019. <https://doi.org/10.1016/j.bpj.2019.10.017>.
35. Lemkul, J. A., S. K. Lakkaraju, and A. D. MacKerell, Jr. 2016. Characterization of Mg²⁺ distributions around RNA in solution. *ACS Omega.* 1:680–688.
36. Roth, A., Z. Weinberg, ..., R. R. Breaker. 2014. A widespread self-cleaving ribozyme class is revealed by bioinformatics. *Nat. Chem. Biol.* 10:56–60.
37. Liu, Y., T. J. Wilson, ..., D. M. J. Lilley. 2014. Crystal structure and mechanistic investigation of the twister ribozyme. *Nat. Chem. Biol.* 10:739–744.
38. Wilson, T. J., Y. Liu, ..., D. M. J. J. Lilley. 2016. The novel chemical mechanism of the twister ribozyme. *J. Am. Chem. Soc.* 138:6151–6162.
39. Panja, S., B. Hua, ..., S. A. Woodson. 2017. Metals induce transient folding and activation of the twister ribozyme. *Nat. Chem. Biol.* 13:1109–1114.
40. Gaines, C. S., T. J. Giese, and D. M. York. 2019. Cleaning up mechanistic debris generated by twister ribozymes using computational RNA enzymology. *ACS Catal.* 9:5803–5815.
41. Ren, A., M. Košutić, ..., D. J. Patel. 2014. In-line alignment and Mg²⁺ coordination at the cleavage site of the env22 twister ribozyme. *Nat. Commun.* 5:5534.

42. Vušurović, N., R. B. Altman, ..., S. C. Blanchard. 2017. Pseudoknot formation seeds the twister ribozyme cleavage reaction coordinate. *J. Am. Chem. Soc.* 139:8186–8193.
43. Draper, D. E. 2008. RNA folding: thermodynamic and molecular descriptions of the roles of ions. *Biophys. J.* 95:5489–5495.
44. Brooks, B. R., C. L. Brooks, III, ..., M. Karplus. 2009. CHARMM: the biomolecular simulation program. *J. Comput. Chem.* 30:1545–1614.
45. Beglov, D., and B. Roux. 1994. Finite representation of an infinite bulk system: solvent boundary potential for computer simulations. *J. Chem. Phys.* 100:9050–9063.
46. Denning, E. J., U. D. Priyakumar, ..., A. D. Mackerell, Jr. 2011. Impact of 2'-hydroxyl sampling on the conformational properties of RNA: update of the CHARMM all-atom additive force field for RNA. *J. Comput. Chem.* 32:1929–1943.
47. Hart, K., N. Foleppé, ..., A. D. Mackerell, Jr. 2012. Optimization of the CHARMM additive force field for DNA: improved treatment of the BI/BII conformational equilibrium. *J. Chem. Theory Comput.* 8:348–362.
48. Jorgensen, W. L., J. Chandrasekhar, ..., M. L. Klein. 1983. Comparison of simple potential functions for simulating liquid water. *J. Chem. Phys.* 79:926–935.
49. Durell, S. R., B. R. Brooks, and A. Bennaïm. 1994. Solvent-induced forces between 2 hydrophilic groups. *J. Phys. Chem.* 98:2198–2202.
50. Essmann, U., L. Perera, ..., L. G. Pedersen. 1995. A smooth particle mesh Ewald method. *J. Chem. Phys.* 103:8577–8593.
51. Ryckaert, J. P., G. Ciccotti, and H. J. C. Berendsen. 1977. Numerical-integration of cartesian equations of motion of a system with constraints - molecular-dynamics of N-alkanes. *J. Comput. Phys.* 23:327–341.
52. Eastman, P., J. Swails, ..., V. S. Pande. 2017. OpenMM 7: rapid development of high performance algorithms for molecular dynamics. *PLoS Comput. Biol.* 13:e1005659.
53. Izaguirre, J. A., C. R. Sweet, and V. S. Pande. 2010. Multiscale dynamics of macromolecules using normal mode Langevin. *Pac. Symp. Biocomput.* 2010:240–251.
54. Virnau, P., and M. Müller. 2004. Calculation of free energy through successive umbrella sampling. *J. Chem. Phys.* 120:10925–10930.
55. Tribello, G. A., M. Bonomi, ..., G. Bussi. 2014. PLUMED 2: new feathers for an old bird. *Comput. Phys. Commun.* 185:604–613.
56. Kumar, S., J. M. Rosenberg, ..., P. A. Kollman. 1995. Multidimensional free-energy calculations using the weighted histogram analysis method. *J. Comput. Chem.* 16:1339–1350.
57. Grossfield, A.. WHAM: the weighted histogram analysis method, version 2.0.9. <http://membrane.urmc.rochester.edu/content/wham>.
58. Sun, D., S. K. Lakkaraju, ..., A. D. MacKerell, Jr. 2018. Determination of ionic hydration free energies with grand canonical Monte Carlo/molecular dynamics simulations in explicit water. *J. Chem. Theory Comput.* 14:5290–5302.
59. Raman, E. P., W. Yu, ..., A. D. MacKerell, Jr. 2013. Inclusion of multiple fragment types in the site identification by ligand competitive saturation (SILCS) approach. *J. Chem. Inf. Model.* 53:3384–3398.
60. MacKerell, A. D., Jr., R. Rigler, ..., W. Saenger. 1987. Protein dynamics. A time-resolved fluorescence, energetic and molecular dynamics study of ribonuclease T1. *Biophys. Chem.* 26:247–261.
61. Hyeon, C., and D. Thirumalai. 2012. Chain length determines the folding rates of RNA. *Biophys. J.* 102:L11–L13.
62. Laidler, K. J. 1987. *Chemical Kinetics*. Harper & Row.
63. Arrhenius, S. 1889. Über die Dissociationswärme und den Einfluss der Temperatur auf den Dissociationsgrad der Elektrolyte. *Zeitschrift für Physikalische Chemie.* 4:96–116.
64. Onoa, B., and I. Tinoco, Jr. 2004. RNA folding and unfolding. *Curr. Opin. Struct. Biol.* 14:374–379.
65. Stofer, E., C. Chipot, and R. Lavery. 1999. Free energy calculations of Watson–Crick base pairing in aqueous solution. *J. Am. Chem. Soc.* 121:9503–9508.
66. Turner, D. H., N. Sugimoto, ..., S. D. Dreiker. 1987. Free energy increments for hydrogen bonds in nucleic acid base pairs. *J. Am. Chem. Soc.* 109:3783–3785.
67. Lilley, D. M. 2012. The structure and folding of kink turns in RNA. *Wiley Interdiscip. Rev. RNA.* 3:797–805.
68. Petrov, A. S., J. C. Bowman, ..., L. D. Williams. 2011. Bidentate RNA-magnesium clamps: on the origin of the special role of magnesium in RNA folding. *RNA.* 17:291–297.
69. Košutić, M., S. Neuner, ..., R. Micura. 2015. A mini-twister variant and impact of residues/cations on the phosphodiester cleavage of this ribozyme class. *Angew. Chem. Int.Engl.* 54:15128–15133.
70. Breaker, R. R. 2017. Mechanistic debris generated by twister ribozymes. *ACS Chem. Biol.* 12:886–891.
71. Draper, D. E. 2013. Folding of RNA tertiary structure: linkages between backbone phosphates, ions, and water. *Biopolymers.* 99:1105–1113.
72. Shiman, R., and D. E. Draper. 2000. Stabilization of RNA tertiary structure by monovalent cations. *J. Mol. Biol.* 302:79–91.
73. Wang, Y., J. M. L. Ribeiro, and P. Tiwary. 2019. Machine learning approaches for analyzing and enhancing molecular dynamics simulations. *arXiv, arXiv:1909.11748* <https://arxiv.org/abs/1909.11748>.
74. Bonneau, E., and P. Legault. 2014. NMR localization of divalent cations at the active site of the Neurospora VS ribozyme provides insights into RNA-metal-ion interactions. *Biochemistry.* 53:579–590.
75. Egli, M., G. Minasov, ..., A. Rich. 2002. Metal ions and flexibility in a viral RNA pseudoknot at atomic resolution. *Proc. Natl. Acad. Sci. USA.* 99:4302–4307.
76. Klein, D. J., T. E. Edwards, and A. R. Ferré-D'Amaré. 2009. Cocrystal structure of a class I preQ1 riboswitch reveals a pseudoknot recognizing an essential hypermodified nucleobase. *Nat. Struct. Mol. Biol.* 16:343–344.
77. Pancera, M., T. Zhou, ..., P. D. Kwong. 2014. Structure and immune recognition of trimeric pre-fusion HIV-1 Env. *Nature.* 514:455–461.